



OPEN ACCESS

EDITED BY

Alessandro Amorosi,
University of Bologna, Italy

REVIEWED BY

Jingrui Li,
Qingdao National Laboratory for Marine
Science and Technology, China
Dongdong Dong,
Chinese Academy of Sciences (CAS),
China

*CORRESPONDENCE

Jing Feng,
✉ fengjing200272@163.com
Haiyan Cheng,
✉ chenghaiyan_2005@163.com

RECEIVED 10 June 2023

ACCEPTED 13 July 2023

PUBLISHED 25 July 2023

CITATION

Jiang S, Dong C, Feng J, Cheng H, Yang J,
Li M, Wang J, Chen X and Zhou Y (2023),
Geological hazards in the Oujiang estuary
in the Zhejiang Province, China: type,
distribution, and origin.
Front. Earth Sci. 11:1237831.
doi: 10.3389/feart.2023.1237831

COPYRIGHT

© 2023 Jiang, Dong, Feng, Cheng, Yang,
Li, Wang, Chen and Zhou. This is an open-
access article distributed under the terms
of the [Creative Commons Attribution
License \(CC BY\)](https://creativecommons.org/licenses/by/4.0/). The use, distribution or
reproduction in other forums is
permitted, provided the original author(s)
and the copyright owner(s) are credited
and that the original publication in this
journal is cited, in accordance with
accepted academic practice. No use,
distribution or reproduction is permitted
which does not comply with these terms.

Geological hazards in the Oujiang estuary in the Zhejiang Province, China: type, distribution, and origin

Shenghui Jiang¹, Chao Dong², Jing Feng^{3*}, Haiyan Cheng^{4*},
Jiaojiao Yang², Meina Li³, Jianqiang Wang², Xuanbo Chen² and
Yubo Zhou²

¹Key Lab of Submarine Geosciences and Prospecting Techniques, MOE and College of Marine Geoscience, Ocean University of China, Qingdao, China, ²Zhejiang Institute of Hydrogeology and Engineering Geology, Ningbo, China, ³Qingdao Institute of Marine Geology, China Geological Survey, Qingdao, China, ⁴Qingdao Geological Exploration Institute of China Metallurgical Geology Administration, Qingdao, China

Introduction: As our understanding of the ocean and its uses continues to advance, countries worldwide with ocean access are implementing new marine strategies. For example, understanding marine geological disasters can help develop the use of ocean resources and oceanic engineering.

Methods: Therefore, this study used recent data from the Oujiang Estuary, a nearshore area in China, to determine its geological hazards.

Results: The geological hazards were classified as active or restricted based on topography, geomorphology, shallow seismic profile, single-channel seismic profile, and geological drilling data. Active geological hazards primarily include shallow gas and active sand waves, whereas restrictive geological hazards include irregularly buried bedrock, erosion channels, steep submarine slopes, and buried paleochannels. We also evaluated the distribution characteristics and scope, such as the vertical distribution of shallow gas based on the seismic profiles, drilling rock facies, methane, and carbon dioxide contents in the top air, and the isotope values. We found that shallow gas was vertically distributed among multiple layers. The main gas-bearing layers were the clayey silt and sandy (silt) clay layers of the early Holocene and late Pleistocene strata. The shallow gas content was relatively low in the coarse sediment layer at the bottom of the late Pleistocene succession. Generally, the Holocene and late Pleistocene deposits do not contain gas, and the gas content in the middle and late Pleistocene strata (at greater depths) is relatively low.

Discussion: The combined effects of the regional geological structure, sea level changes, modern hydrodynamics, and human activities have formed the geological environment of the Oujiang Estuary.

KEYWORDS

oujiang estuary, geological hazards, shallow gas, origin, marine structures

1 Introduction

Marine geological hazards are an important research branch in the geological hazards field, becoming a marginal discipline with the exploration and development of nearshore oil and gas and seabed mineral resources (Wang et al., 2014; Feng et al., 2017; Qiao et al., 2022). Marine geological disasters are phenomena or events caused by external geological effects, such as waves, ocean currents, and storm surges, or internal geological effects, such as earthquakes, faults, and volcanic activities, threatening human life and property (Ye, 2011; Liu et al., 2014; Qiu et al., 2018).

Marine geological hazards can be classified in many ways but are generally deemed active or restricted based on the activity level of the potential geological hazards (Bao and Jiang, 1993; Sun et al., 2010; Chen S. et al., 2020). Active geological hazards can move, causing direct damage to marine engineering and the natural environment under internal and external forces, such as shallow gas, pockmarks, submarine landslides, active faults, active sand waves, liquefaction of sand and soil, bottom heave, coastal erosion and accretion, and landslides. Restricted geological hazards, also called restrictive geological conditions, cannot move; instead, they restrict certain marine engineering projects. If ignored, they pose hidden dangers in marine engineering. Examples include buried paleochannels, depressions, steep underwater slopes, irregularly shallow buried bedrock, and troughs.

The Oujiang Estuary is situated along the coast of Wenzhou City in Zhejiang Province, China, and is one of the most important river mouths in the region, with more than 200 large and small islands in the estuary area. This region is rich in marine resources, including ports, tidal flats, fisheries, and tourism, making it a key area for economic development. However, the area's marine geological environment is complex and influenced by various dynamic conditions, including Oujiang River runoff, waves, tides, and currents, resulting in the formation of a series of shoal-channel geomorphic systems in the coastal area outside the estuary that hold potential for various geological disasters. Therefore, this study investigated the marine geological hazards in this area to provide basic data for further studies of marine environmental evolution, ocean development, and ocean engineering construction (Yang et al., 2022).

2 Materials and methods

2.1 Geological setting

The Oujiang Estuary is in the central part of the Wenzhou metropolitan area and is its main axis, situated between the Yangtze River Delta and Pearl River Delta economic zones in the northern part of the West Coast Economic Zone (Zhang et al., 2020). It is also located at the intersection of the middle section of the Yellow Sea coastline and the Oujiang golden waterway “T.” The nearshore terrain of the Oujiang Estuary is relatively complex, with many islands in the region, dense shoals, and intersecting shoal channels. River erosion and tidal currents mainly affect the section within the estuary. The northern mouth of the Oujiang River is more strongly eroded than the southern mouth, with a water depth generally less than 15 m, while the southern mouth has a water depth of generally less than 10 m; the average depth is approximately 7–8 m (Shang et al., 2018). The section outside the mouth of the estuary is affected by open terrain, island reef distribution, and tidal erosion, resulting

in considerable changes in the terrain, with strong tidal currents between the islands. Generally, a good waterway forms when the depth is more than 20 m, and sediment accumulates around the waterway, forming shoals in some local areas. The terrain is generally less than 5 m deep, with isobaths developing around the islands.

This area is in the Southeast Zhejiang Uplift of the South China Fold Belt, which has been an active continental margin since the Mesozoic period, manifesting as strong fault movement and large-scale calc-alkaline magmatic activity. The fault structure is highly developed, with dominant regional deep and large faults oriented in the northeast and northwest directions, constituting the basic structural framework of this area (Xu et al., 2007).

2.2 Seismic profiles and boreholes

Shallow- and single-channel seismic profiles were acquired for the Oujiang Estuary in 2017 and 2018 (Figure 1). Shallow seismic profiles were obtained using a sub-bottom profiling high-resolution acoustic system (AAE Technologies, Great Yarmouth, United Kingdom) with an electric spark source as the seismic source. Single-channel seismic measurements were conducted using a G.I air gun with a maximum source capacity of 210 in³ (Sercel, Carquefou Cedex, France), and the receiving cable was a SIG model 16.48.65 receiving cable (SIG, Bouvron, France). Before the marine geophysical survey, method-related and technical experiments were conducted in the Oujiang Estuary. The parameters for the shallow seismic profile were experimentally determined, including the excitation energy (typically selected at 800 J), band-pass filtering (100–5000 Hz), and the timely adjustment of seabed tracking (based on the strength of the reflection signal). The data were recorded in SGY format with a printing range of 200 ms. The parameters for the air gun operations were: source capacity: 90 in³; air pressure: 1600–1800 psi; streamer drag length: 40 m; and source drag length: 35 m. Seabed tracking was promptly adjusted based on the strength of the reflection signal, and the data were recorded in the SGY format with a recording range of 500 ms. The seismic profiles of the study area were interpreted based on recognition markers of the seismic reflection interfaces. The distribution patterns were determined by identifying the characteristics and ranges of various geological factors of disasters in the seismic profiles based on their reflection features.

2.3 Core data and chart data collection

In 2019, two geological boreholes, DSJ3 and DSJ4, were drilled along the seismic profile using an XY-2 drilling rig and the rotary sampling method (Figure 1). DSJ3 reached a depth of 200.3 m, with an average recovery rate of 95.54% in the mud layer and 90.74% in the sand layer. DSJ4 reached a depth of 182.9 m, with an average recovery rate of 95.52% in the mud layer and 83.68% in the sandy layer. The recovered rock cores were then stored in a laboratory for photography, preservation, description, and sampling. Intact shells were selected from the cores for accelerator mass spectrometry ¹⁴C dating at Beta Analytic (Miami, FL, USA). Grain size and paleomagnetic samples were collected at approximately 30–35 cm intervals. Grain size analyses were completed at the China University of Geosciences, whereas paleomagnetic testing was conducted at the East China Mineral Resources Supervision and Testing Center of the Ministry of Natural Resources.

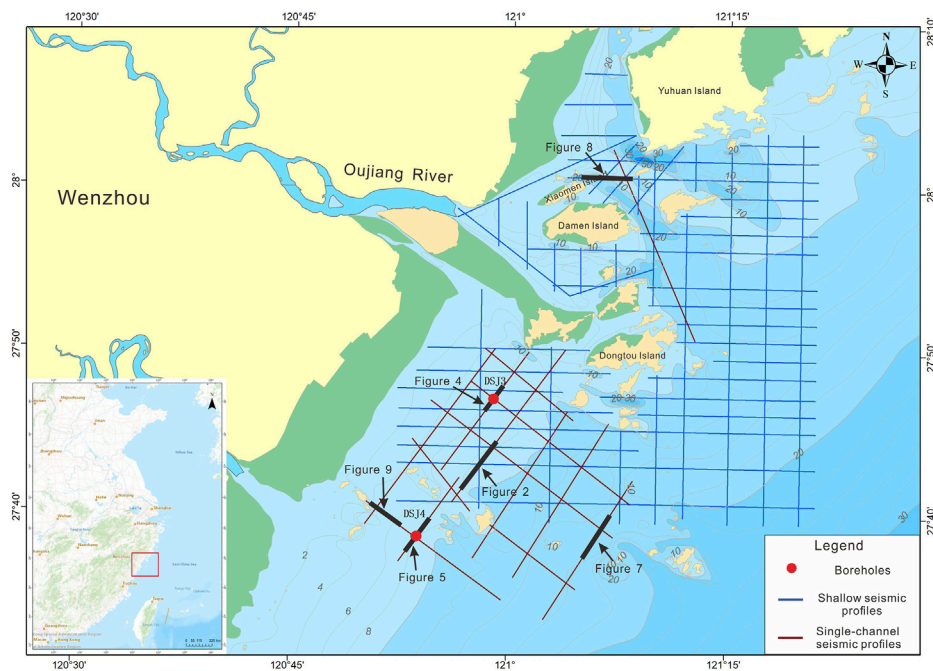


FIGURE 1
Seismic profile and borehole locations in the Oujiang Estuary offshore area. Red circles represent boreholes, blue lines represent shallow seismic profiles, and red lines represent single-channel seismic profiles.

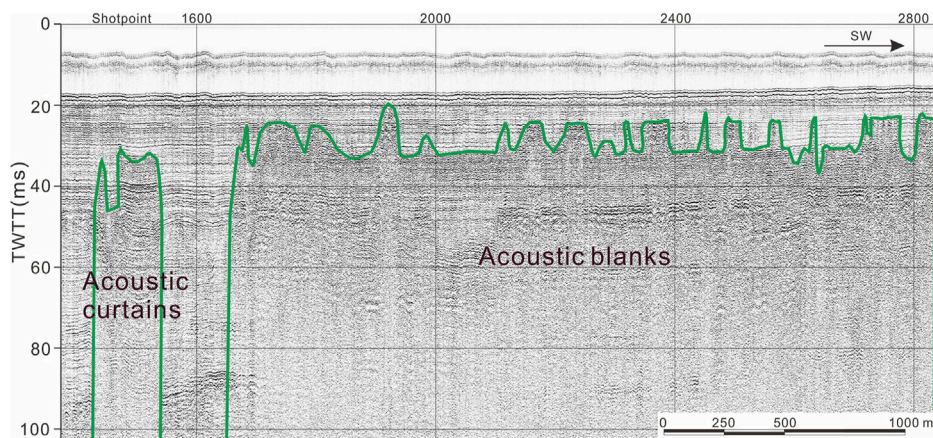


FIGURE 2
Acoustic blanks, acoustic curtains, and acoustic disturbance from the shallow seismic profile in the Oujiang Estuary. SW: Southwest; TWTT: Two-way travel time.

Chart data were collected from four historical datasets from 1979, 1986, 2002 and 2011 to reflect the morphological evolution of active sand waves according to changes in water depth.

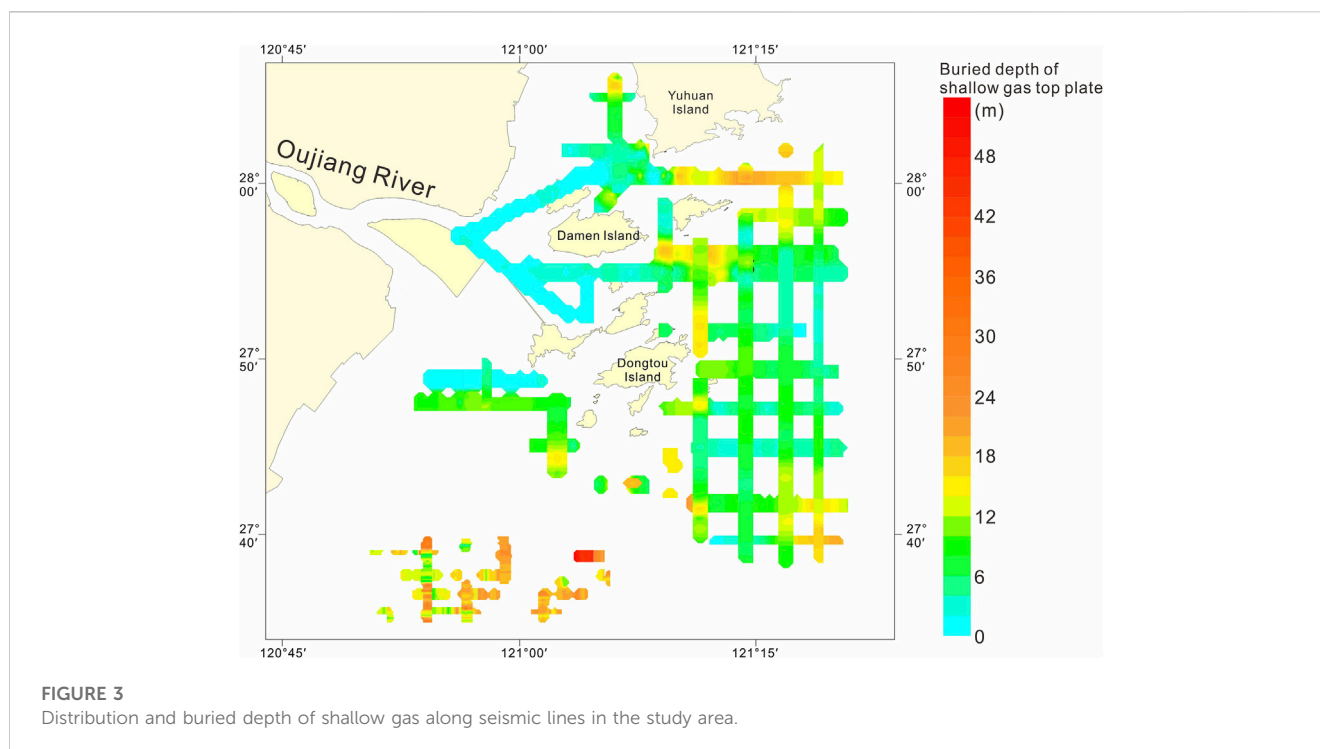
3 Results

The geological hazards in the study were classified as active or restricted based on the degree of geological activity of the potential hazards.

3.1 Active geological hazards

3.1.1 Shallow gas

In the sedimentary succession, gas can decrease the seismic wave propagation velocity and cause rapid attenuation of the reflected wave energy, resulting in little or no energy reflection (Benites, et al., 2015). This event forms a “reflection blurry zone,” shielding sedimentary reflection information. Seismic reflection characteristics mainly manifest as “acoustic blanks,” “acoustic



curtains,” “acoustic disturbances,” and other phenomena (Figure 2). If shallow gas escapes from the seabed, it can form special micro-landforms, such as “pockmarks” and “mud volcanoes” on the seafloor (Dondurur et al., 2011; Chen Y. et al., 2020). Thus, the shallow gas feature results of the area were projected onto a plane to obtain the shallow gas distribution and burial depth of the top plate (Figure 3). The study area had a widespread distribution of shallow gas in the sea, and the distribution had relatively evident regional variation, mainly distributed northeast of the study area. The burial depth of a shallow gas top plate is generally between 5 and 30 m, but mostly within 12 m, with a maximum burial depth of over 50 m. The burial depth of the shallow gas in the southwest region of the study area was relatively large, ranging from 3 to 52 m, whereas the burial depth in the northeast region was generally shallow, with a maximum burial depth of approximately 30 m. No obvious seafloor “pockmarks” were observed on the seismic profiles in the study area, indicating that shallow gas did not overflow, or the overflow was minimal, and it was not enough to affect the micro-landform morphology.

The vertical distribution characteristics of shallow gas at the drilling site were obtained based on the seismic profiles, core samples, and methane (CH₄) content in the top air and interstitial water samples. The seismic profile of the DSJ3 borehole revealed that the gas-bearing top plate of the shallow gas was approximately 12 m, and the CH₄ content in the top air sample was almost zero at a depth of 11 m or less, consistent with the analysis results of the two (Figure 4). The lithology of this section is silty clay, corresponding to the middle-late Holocene succession. Within a depth range of approximately 11–100 m, the deposits are generally gas-bearing, corresponding to the early Holocene and late Pleistocene strata. The shallow gas content is roughly divided into three sections: 1) 11–43 m, relatively high gas

content and corresponding to the clayey silt layer of the Holocene and late Pleistocene; 2) 43–80 m, low content of gas; and 3) 80–100 m, a small or non-existent gas content in the coarse sediment layer, such as the medium-fine sand layer.

An obvious “reflection blurry zone” was not observed at the DSJ4 location, but the seismic profile revealed a more obvious “reflection blurry zone” approximately 500 m southeast along the seismic profile (Figure 5). The buried depth at the top of the blurry zone was consistent with the buried depth of the CH₄ content greater than zero in the top air sample. Moreover, the overall CH₄ content at DSJ4 was lower than that at DSJ3 based on the content in the top air sample. Therefore, DSJ4 likely has a low shallow gas content, reflected in the single-channel seismic profile of the air gun. Furthermore, the CH₄ content was the highest in the clayey and sandy silt deposits of the early Holocene and late Pleistocene, with a burial depth of approximately 27–75 m. In strata deeper than 75 m, the CH₄ content was generally low.

Based on the borehole data, shallow gas was vertically distributed among multiple layers. The main gas-bearing layers were the clayey silt and sandy (silt) clay layers of the early Holocene and late Pleistocene strata. The shallow gas content in the coarse sediment layer at the bottom of the late Pleistocene deposits was relatively low. Generally, the Holocene and late Pleistocene strata do not contain gas, and the gas content in the middle and late Pleistocene deposits at greater depths is relatively low. Based on the engineering characteristics of the drilling sample analyses, the main gas-bearing rock types were clayey silt and silty clay layers, which are not conducive to the large-scale storage and accumulation of gas. Also, the gas pressure and volume were generally low. The single-channel seismic results did not reveal the “pockmark” phenomenon on the seafloor, indicating that shallow gas did not overflow or the overflow was small; thus, it

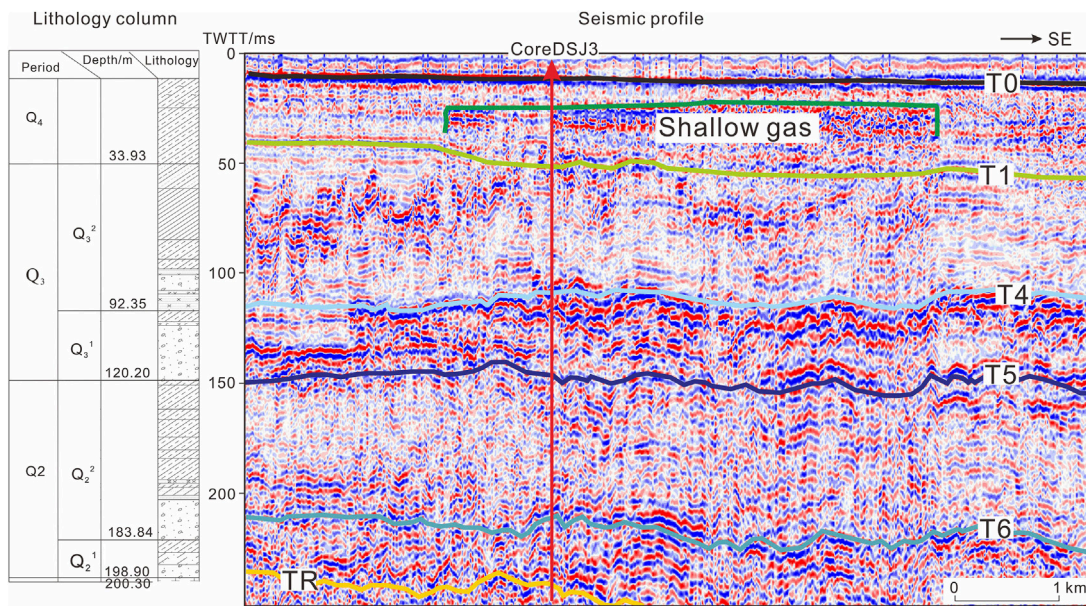


FIGURE 4 Comparisons between the single-channel seismic unit division and core DSJ03 lithology. SE: Southeast.

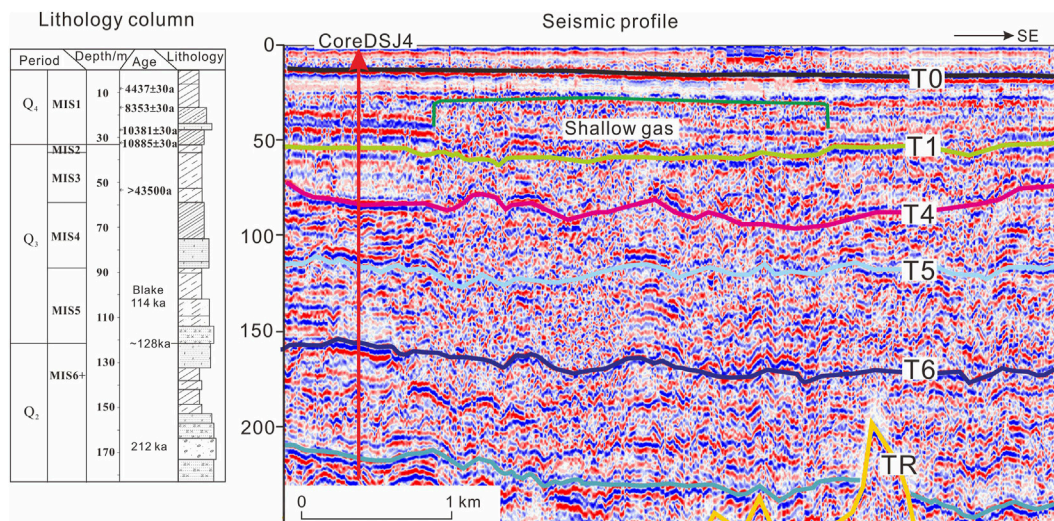


FIGURE 5 Comparisons between the single-channel seismic unit division and core DSJ04 lithology. SE: Southeast.

was not enough to affect the micro-geomorphic features. Most of the gas was isolated from the viscous soil layer in the form of small bubbles. Overall, the possibility of a large-scale blowout in the study area is believed to be low; however, the possibility of locally high instantaneous gas pressure cannot be excluded.

3.1.2 Active sand waves

Larger-scale active sand waves in the study area were mainly distributed in the shallow sea area of the northern mouth of the

Oujiang River, the west side of the Damao Island’s triangular sand, the Zhongsha and Chongshan sand waves on the south side, and sporadically distributed in the Qitouyang Sea area at the southern mouth of the Oujiang River (Figure 6). Among these, triangular sand wave was the largest in scale, with a triangular shape resembling a horseshoe. During low tide, shallow sand waves were exposed, which extended in two directions, northwest and southeast, and were mainly composed of medium-to fine-sand sediment. In recent years, the sand waves have eroded near the river mouth, the

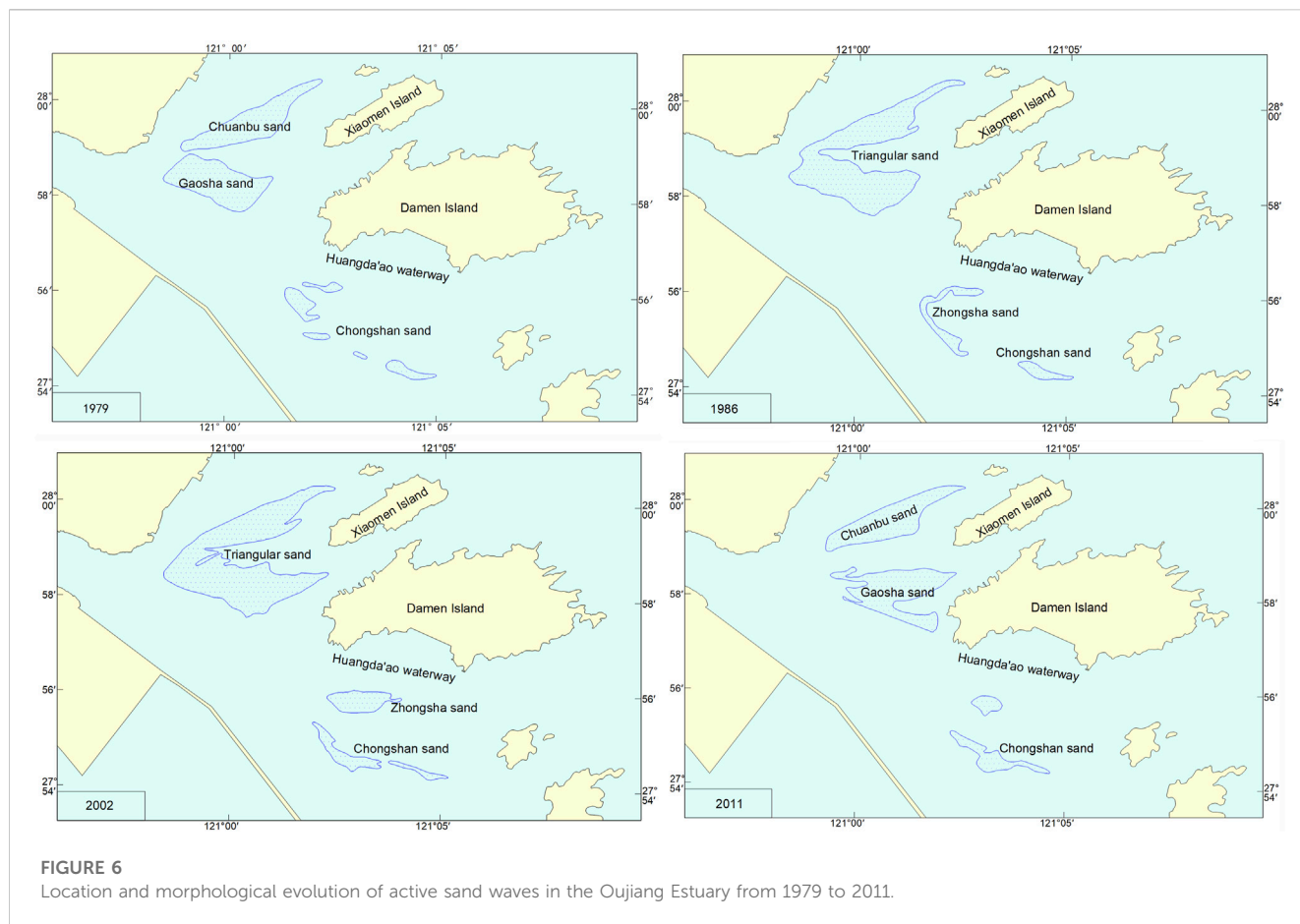


FIGURE 6 Location and morphological evolution of active sand waves in the Oujiang Estuary from 1979 to 2011.

TABLE 1 Active sand wave changes from 1979 to 2011 (km²).

Active sand waves	Year			
	1979	1986	2002	2011
Triangular sand	9.36	10.99	12.86	10.14
Zhongsha sand	1.16	1.34	1.64	0.58
Chongshan sand	0.89	0.64	1.59	1.54

terrain has deepened, the 0 m line range has shrunk, and the tidal current has cut through the middle of the sand wave, dividing the triangular sand into Chuanbu sand and Gaosha sand waves.

On a smaller scale, the Zhongsha and Chongshan sand waves are located on the southern side of the Huangda'ao Waterway. Since 1979, Zhongsha gradually formed from a series of smaller-scale tidal sand bodies, with southeastern and northwestern axis lengths of 2.6 km and 2.3 km, respectively. In recent years, owing to the completion of the Lingni Dyke, the range of the mid-water channel has narrowed, the main axis of the tidal current has shifted northward, the flow rate has increased, and the shallow water of Zhongsha has eroded, and by 2011, the 0 m line continued extending toward the Chongshan sand wave, and the southern end of Zhongsha merged with Chongshan sand (Table 1). Therefore, the Chongshan sand wave scale expanded and continued to develop.

3.1.3 Erosion channels

Natural erosion and scouring of surface sediments on the seabed form erosion channels, which are mainly distributed in narrow areas between islands with strong tides or water currents. Steep channels are often accompanied by steep slopes prone to landslides. Waterways are large channels that serve as water transportation routes and play an important role in local economic development. However, there are significant constraints on certain offshore engineering projects, such as laying submarine cables and oil pipelines. Erosion channel slopes are generally steep, which can easily cause sediment on the slope to collapse, undermining the foundation of buildings and causing pipelines, cables, and other structures to break or deform. Therefore, erosion channels pose a hidden danger to offshore engineering construction.

Erosion channels are identifiable from a single seismic profile and were the main topographic features in the study area. They were characterized by deep-cut channels and a generally small-scale distribution, mainly located in tidal channels between the islands (Figure 7).

3.2 Restricted geological hazards

3.2.1 Irregular shallow-buried bedrock

In a single seismic profile, bedrock is mainly characterized by medium to low frequency, strong amplitude, and medium to low

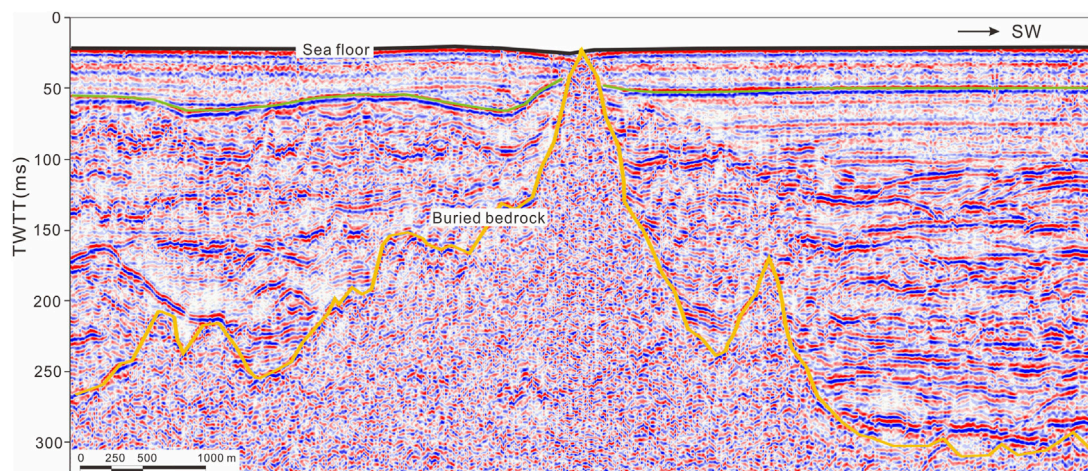


FIGURE 7
The single-channel seismic profile reveals irregular shallow buried bedrock. SW: Southwest; TWTT: Two-way travel time.

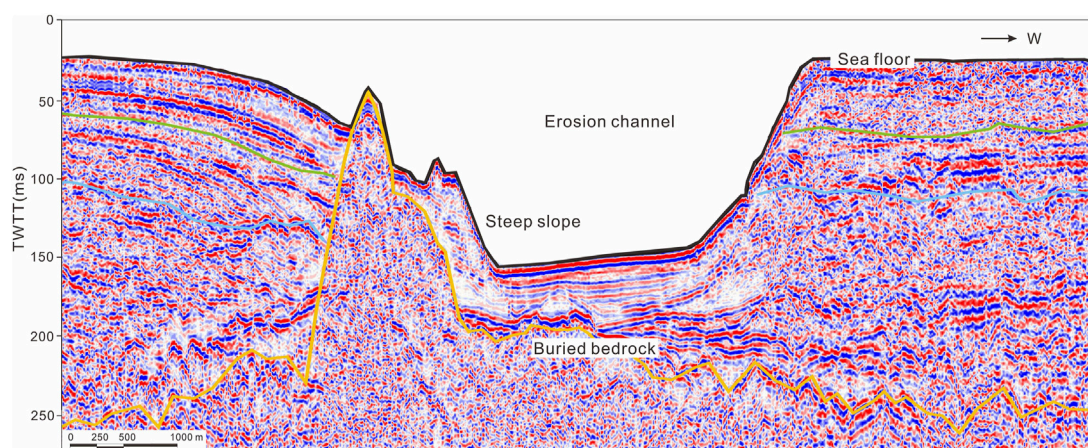


FIGURE 8
The single-channel seismic profile reveals irregular shallow buried bedrock, steep slopes, and erosion channels. TWTT: Two-way travel time; W: West.

continuity reflection features. We identified irregular reflection morphology with high and low undulations, and the bedrock surface protrusions often exhibited strong reflections in the form of conical or pointed peaks (Figure 8). Also, the internal reflections were blurry and chaotic, with no clear layering, and some diffraction waves were observed. The shallow bedrock in the study area mainly appeared in areas close to the bedrock coast and islands, with limited regional distribution. Bedrock outcrops in some local sea areas became reefs and were primarily distributed in areas with large seabed undulations. In this study, in a single seismic profile, we observed 11 bedrock outcrops ranging from 3.5 to 28.5 m in depth.

3.2.2 Steep submarine slopes

Steep submarine slopes are large and prone to instability and landslides/tipping under external disturbances, potentially

causing catastrophic consequences for underwater facilities, such as underwater pipelines, cables, pipe networks, and anchorages, and is a safety hazard for submarine slope stability (Wang et al., 2019).

Steep submarine slopes have distinguishing features in the data, such as in a single seismic profile and depth measurements. Steep slopes are usually characterized by an intensive arrangement of terrain contours, and their linear shapes and positions can be clearly seen on three-dimensional topographic maps. Single seismic profiles mainly manifest as significant distortions of the seabed reflection waveform or sudden changes in water depth. Based on the characteristics of steep slopes in the Wenzhou Sea, slopes greater than 6° were defined as submarine steep slopes. The study area is densely populated, with islands and waterways prone to forming deep trench-shore slopes. Therefore, the steep slopes in the study area were mainly erosion-steep

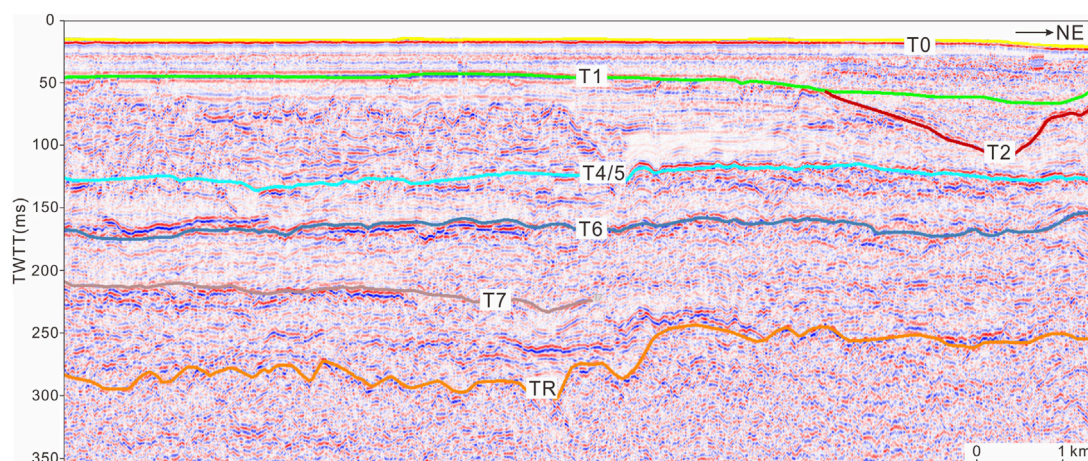


FIGURE 9

The single-channel seismic profile reveals a late and middle Pleistocene paleo-channel. Note: [Figure 1](#) shows the location of the profile. NE: Northeast; TWTT, two-way travel time. T0-T7: seismic interfaces. TR: bedrock.

slopes, and their extension direction was consistent with the direction of the isobaths. In total, 59 steep submarine slopes were identified through a single seismic survey, with slopes $>6^\circ$. The maximum slope was 20.8° , and the steep submarine slopes in the study area were distributed on both sides of the scouring grooves in the tidal channels between the islands ([Figure 8](#)).

3.2.3 Buried paleo-channel

In a single seismic profile, buried paleochannel sediments show various types of reflections, such as complex wave-like cluttered reflections, sub-parallel reflections, high-angle inclined interlaced reflections, and pre-fill reflections at different angles, some of which can be subdivided into multiple filling stages cut by each other ([Qiu et al., 2012](#)).

A comparative analysis of single-channel seismic interpretation results and drilling data suggests that three periods of paleo-channels have developed in the survey area since the early Pleistocene period ([Figure 9](#)). The locally developed late Pleistocene paleo-channel (T2 interface) extends towards the south of the Oujiang Estuary. The single-channel seismic profile cut down the lower marine succession as a basement, with internal reflections exhibiting subparallel and progradational reflections. The ancient early-late Pleistocene river channel (T6 interface) has been extensively developed on a larger scale. In the single-channel seismic profile, the basement was a strongly eroded interface with local fluctuations showing downward erosion and internal reflections exhibiting sub-parallel, chaotic, and oblique-cross reflections. In the drilling logs, the filling layers inside the paleo-channel demonstrate the basic characteristics of fluvial facies with an upward vertical fining trend. The ancient late-middle Pleistocene river channel (T7 interface) was widely developed. In the single-channel seismic profile, the basement is a strongly eroded interface identifiable by fewer overall fluctuations, whereas the internal reflections exhibit subparallel, chaotic, and oblique cross reflections. In the drilling logs, the filling layers inside the paleo-channel demonstrated the basic characteristics of fluvial facies with an upward vertical fining trend.

4 Discussion

Geological hazards in the study area result from geological structures and various external dynamic forces. Geological structures determine and influence the overall pattern of modern land-sea interactions and the distribution of coastal morphology and types. Thus, various external forces shape modern landforms, which, in turn, affect the types and scope of the geological hazard distribution ([Figure 10](#)).

4.1 Regional geological structure

The Wenzhou region is in the southeastern part of the Zhejiang Province, and the regional geological structures of this area have undergone long and complex processes to become their current form ([Wang et al., 2010](#)). Overall, two different structural systems control the landform in this area: the north-northeast and northwest directional structural systems ([Figure 11](#)). The north-northeast faults control the uplift of the western area to form high mountains and V-shaped valleys and control the formation of plain terrain in the east since the Quaternary period. Specifically, the main structural framework is composed of the Wenzhou-Zhenhai deep fault in the north-northeast, the Pingyang-Putuo deep fault, the Chun'an-Wenzhou major fault in the northwest, and the Taishun-Huangyan major fault in the northeast, which affect the area via volcanic activity, magma intrusion, and the formation and development of sedimentary basins.

4.2 Sea level change

Large-scale sea transgression and regression also cause significant fluctuations in the shoreline and have important influences on the formation of modern coastal morphology and changes in hydrodynamic conditions, material sources, and sedimentary environments. Since the late Pleistocene period, the

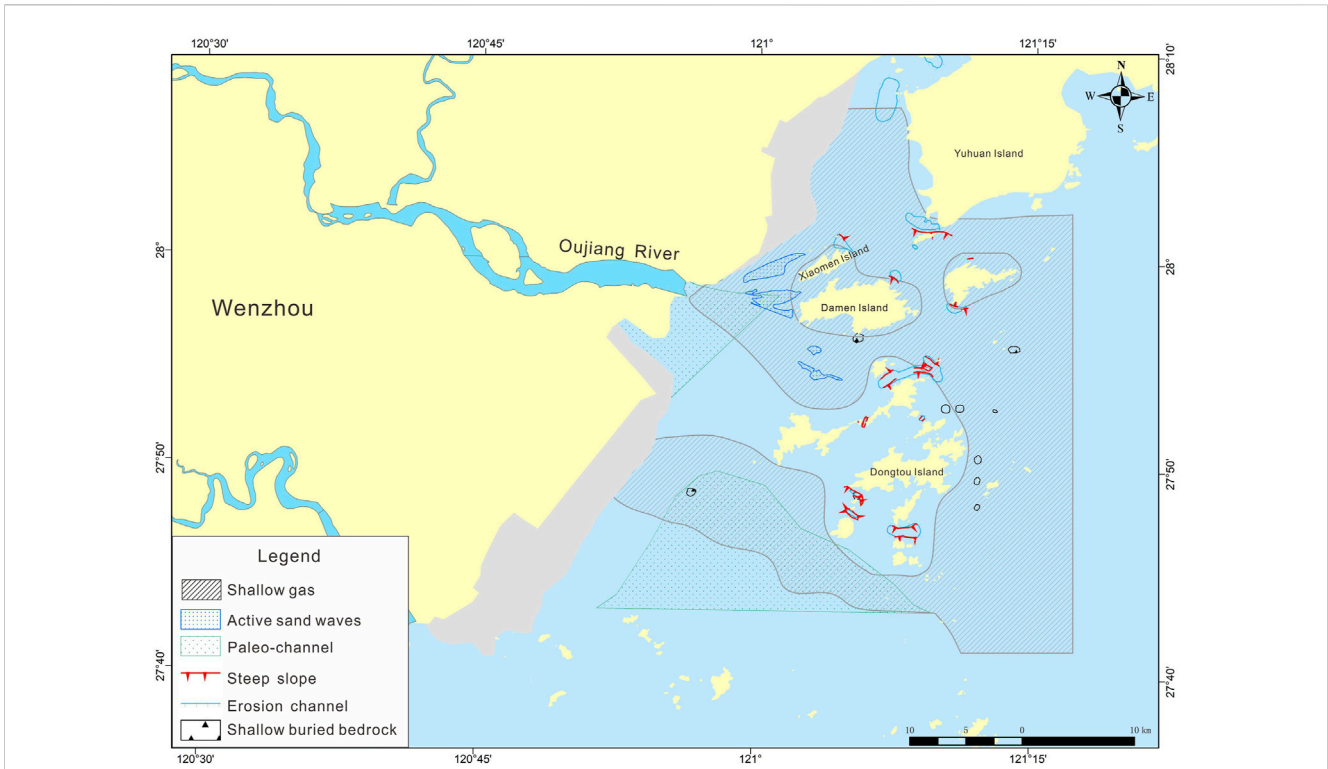


FIGURE 10
Geographical hazard map of the Oujiang Estuary.

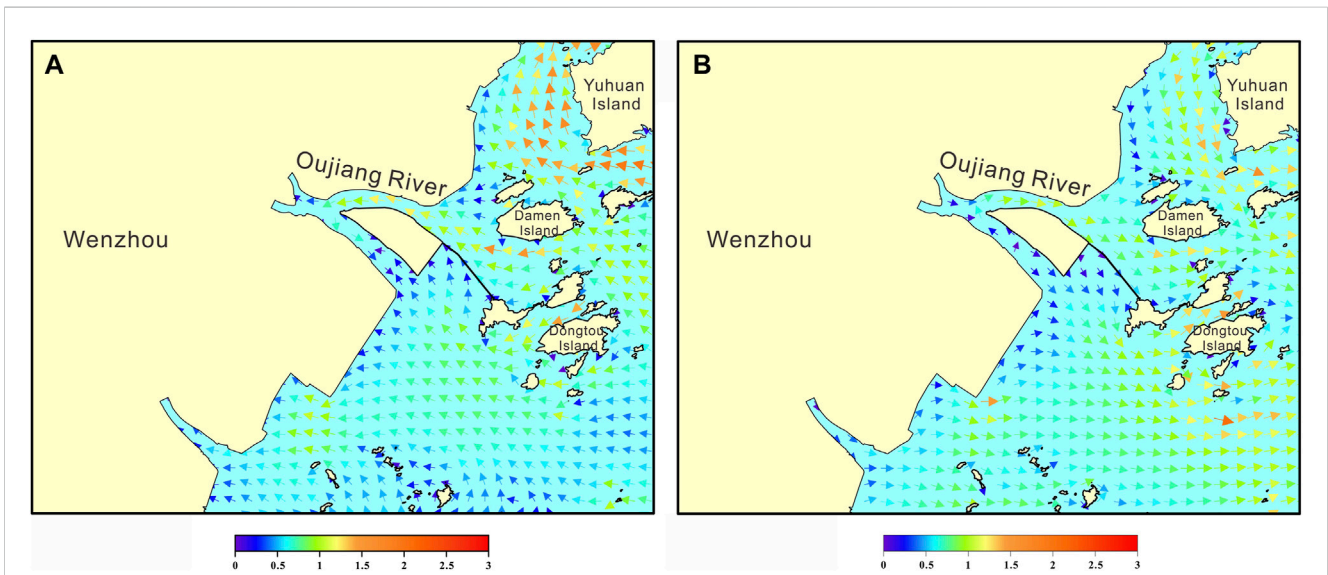
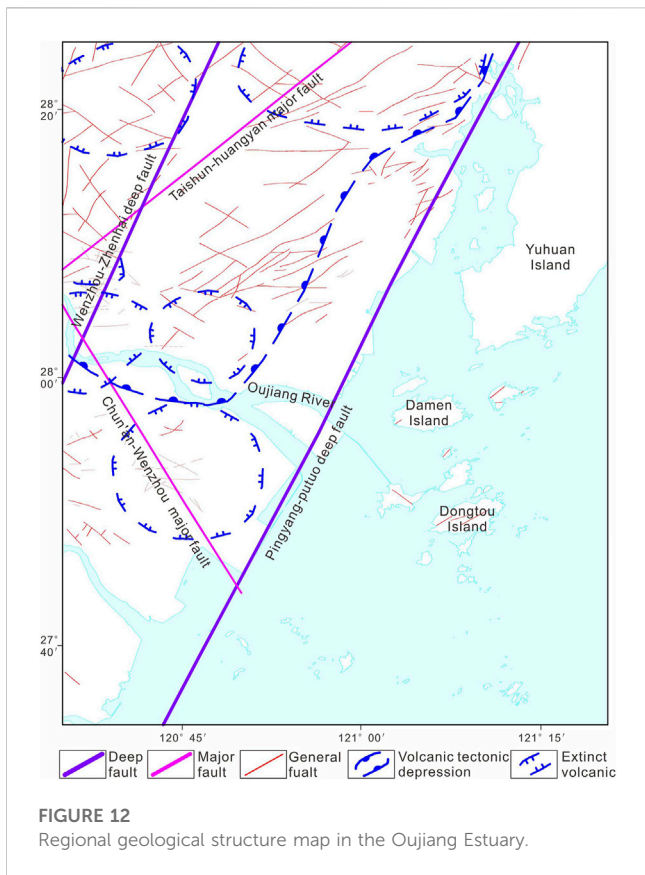


FIGURE 11
Local tidal current fields in the Oujiang River estuary at maximum flood (A) and ebb (B) moment (spring tide) (unit: m/s).

sea level in the Wenzhou coastal area has fluctuated, gradually stabilizing towards its current state during the middle Holocene period. The rise and fall of the sea level have caused constant erosion, transportation, and sedimentation accumulation in the paleo-channel and the seabed active sand waves, affecting the

morphological evolution of the paleo-channel, active sand waves, and erosion gullies.

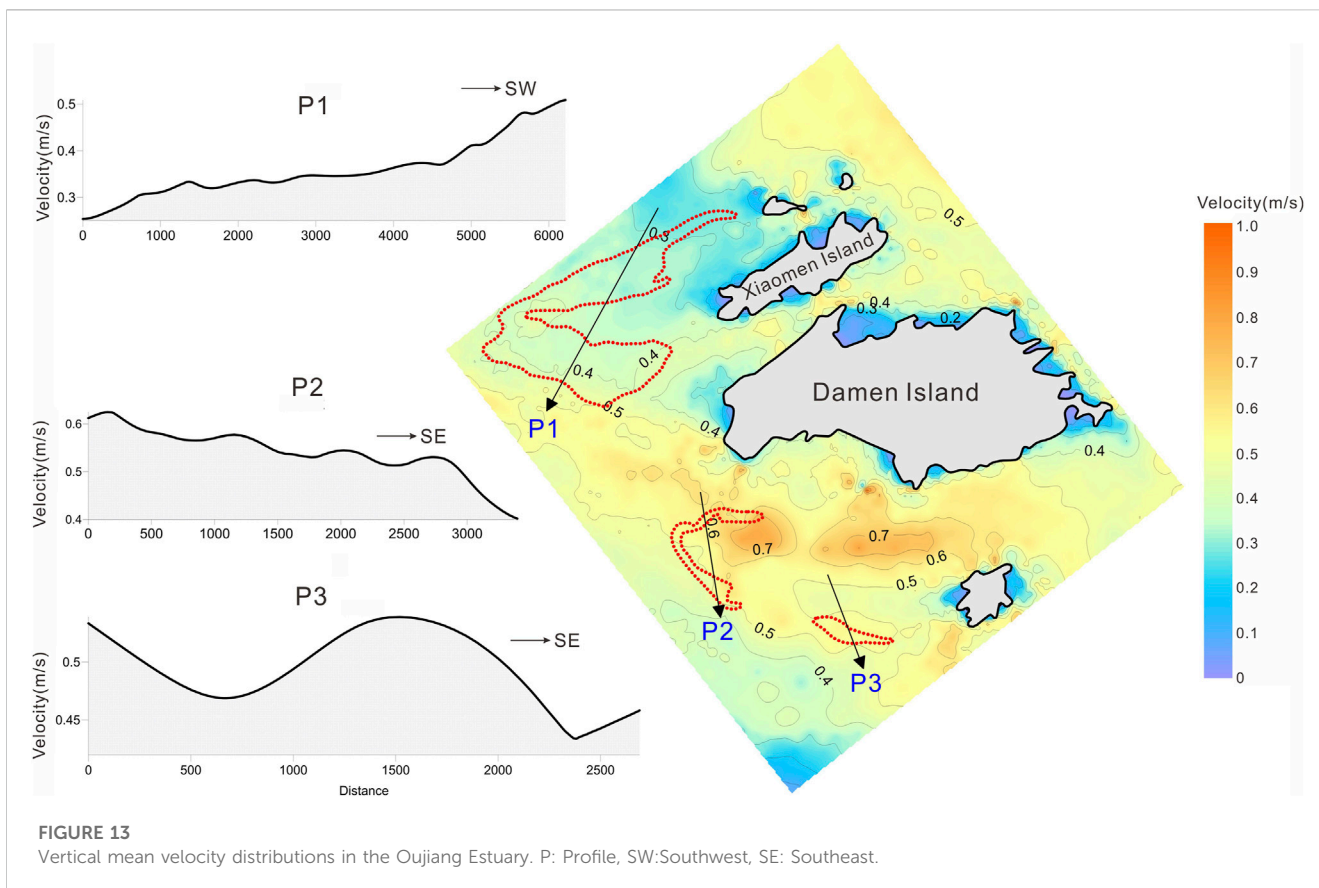
In addition, abundant amounts of terrestrial organic matter within the overlying fill of the paleo-channel have been buried by allochthonous sediment owing to the frequent sea level changes;



consequently, oxygen isolation has occurred, and a rapid transition to a reduced environment is possible. Additionally, sediment cover-layers act as traps for dissolved substances that supply organic matter, which, in its immature stage, is biochemically decomposed by anaerobic bacteria to produce methane or biogas, commonly associated with shallow gases in paleo-channels. Based on its genesis, shallow gas can be divided into two types: biogenic and thermogenic gas (Zhang et al., 2008; Toth et al., 2014). Biogenic gas is formed by organic matter in shallow deposits under anoxic conditions through bacterial reduction. Thermogenic gas is formed by the thermal decomposition of organic matter in deep strata, often in a supercritical state (high-pressure gas chamber), that sometimes rises, migrating and accumulating as shallow gas along rock pore spaces, fissures, and fault planes. In recent years, most domestic and foreign experts have used an $\delta^{13}C_1$ value of less than -55‰ as the empirical characteristic boundary value to distinguish between biogenic, thermogenic, and sub-biogenic gas methane carbon isotopes (Verweij et al., 2018). However, our isotope analysis of the DSJ3 and DSJ4 wells indicated that the $\delta^{13}C_1$ values were between -97.69‰ and -70.74‰ , suggesting that the shallow gas in the study area is a typical biogenic gas generated through a CO_2 reduction reaction (Weschenfelder et al., 2016).

4.3 Modern dynamics

Based on tectonic movement and sea level changes, modern marine dynamic conditions, such as rivers, waves, currents, and



tides, continually reshape and construct topography and are important factors controlling dynamic changes in topography and sediment sources (Figure 12). The development and evolution of the Oujiang Estuary coastal zone topography are continually influenced by the combined action of river inflow, nearshore circulation systems, and wave and tidal forces and play a significant role in the dynamic adjustment of active geological hazards (Wu et al., 2018).

The area had an extensive tidal range and fast flow, forming a typical tidal sandbody. Based on the tidal flow data measured on site from the Oujiang Estuary, which has active sand waves, the discriminant coefficient of the tidal flow was <0.5 , indicating an irregular semidiurnal shallow sea tidal flow (Figure 13). Tidal waves are generally controlled by the M2 tide with a semidiurnal tidal current; the direction of the flood flow is northwest, whereas the ebb flow direction is southeast. Based on the tidal flow velocity distribution, the average tidal flow velocity in the triangular sand area was generally 0.3–0.4 m/s (Liu and Xia, 2007). In addition, the flow velocity in the sand wave area from north to south increased gradually and was generally <0.5 m/s. Finally, the average tidal flow velocity was generally 0.5–0.7 m/s in the middle sand and Zhongshan sand wave areas, and the rising flow velocity was slightly lower than the ebb flow velocity (Zhuang et al., 2008; Ye et al., 2016). Based on sediment grain size data in the sand wave area, the median grain size of sediment that makes up the sand waves was 0.30–0.42 mm, classified as medium sand. The sediment particles in the study area can be transported under the action of tidal current, resulting in higher mobility of sand waves.

4.4 Human activity

Human activity is an inevitable factor in the evolution of geological hazards. In recent decades, with the continuous social economic development, existing land resources have limited further development of Wenzhou City. The government has shifted its focus to the Oujiang Estuary, actively implementing development and remediation projects, such as enclosing and channel construction. Wenzhou City has completed projects such as the Ou-Fei Shoal partial enclosure, Zhaoyuanao harbor area partial enclosure, Wenzhou Shoal enclosure phase 1, Xiaomen Island northern enclosure, Dameng Island Huangao enclosure, and Dongtou Islands enclosure. High-intensity coastal engineering development and other human activities have altered the local hydrodynamic action and sediment deposition balance, causing disturbances in natural geological processes and ultimately leading to the formation, development, and evolution of marine geological disasters (Zhang et al., 2020).

The Wenzhou Shoal Enclosure Project commenced in 2003 (Zheng, 2010). The first phase of the project, Lingni Dike, located along the northern edge of Wenzhou Shoal, was completed and opened to traffic in 2006. The dike effectively intercepted the suspended sediment transport pathway between Wenzhou Shoal and the Middle Channel, leading to a predominantly oscillating flow in the tidal currents of both channels (Xu et al., 2017). Within this interaction, various degrees of slow flow, diversion, and convergence exist, resulting in the complexity of tidal

channel fluctuations and the diversity of sediment erosion and deposition at the mouth of the Ou River, ultimately leading to the amalgamation of Zhongsha Shoal and Chongshan sand wave due to erosion and migration (Figure 6).

5 Conclusion

The main geological hazards in the Oujiang Estuary include shallow gas, active sand waves, shallow-buried irregular bedrock, erosion channels, steep submarine slopes, and buried paleochannels. The seismic profiles and borehole data revealed the vertical distribution characteristics of the shallow gas; the main gas-bearing layers in the early Holocene and late Pleistocene strata were clayey silt and silt (sand) clay layers, and the shallow gas content in the coarse sedimentary layer at the bottom of the late Pleistocene was relatively low. There was no gas content in the middle-late Holocene succession, and the gas content in the deep middle Pleistocene succession was relatively small.

Moreover, the hazardous geology in the study area resulted from the geological structure and various external dynamic forces. The geological structure determines and influences the overall pattern of modern land and sea and the distribution of coastal contours and types. Various external forces (including sea-level changes, modern hydrodynamics, and human activities) have shaped modern landforms, affecting the distribution and evolution of hazardous geology.

Data availability statement

The original contributions presented in the study are included in the article/supplementary material, further inquiries can be directed to the corresponding authors.

Author contributions

SJ and CD contributed to conception and design of the study. JF and YZ organized the database. JY performed the statistical analysis. HC and SJ wrote the first draft of the manuscript. SJ, JW, and XC wrote sections of the manuscript. All authors contributed to the article and approved the submitted version.

Funding

This study was funded by the Comprehensive Geological Survey of Key Coastal Zone in Zhejiang Province (Wenzhou Key Area) (No. 2018009) and Shandong Provincial Natural Science Foundation (No. ZR2021MD049).

Conflict of interest

The authors declare that the research was conducted in the absence of any commercial or financial relationships that could be construed as a potential conflict of interest.

Publisher's note

All claims expressed in this article are solely those of the authors and do not necessarily represent those of their affiliated

organizations, or those of the publisher, the editors and the reviewers. Any product that may be evaluated in this article, or claim that may be made by its manufacturer, is not guaranteed or endorsed by the publisher.

References

- Bao, C., and Jiang, Y. (1993). Types and characteristics of potential subbottom geological hazards in nearshore zone of China. *Trop. Oceanol.* 18 (3), 25–31.
- Benites, M., Alves, D. P., Maly, M. D., and Jovane, L. (2015). Shallow gas occurrence in a Brazilian ria (Saco do Mamanguá, Rio de Janeiro) inferred from high-resolution seismic data. *Cont. Shelf Res.* 108, 89–96. doi:10.1016/j.csr.2015.08.022
- Chen, S., Wang, Z., Zhang, Y., Zhang, Z., Zhao, W., and Zhong, W. (2020a). Characteristics and origin of disaster geological bodies in the northern outer shelf of the East China Sea and its adjacent areas. *Geol. China* 47 (5), 1512–1529.
- Chen, Y., Deng, B., and Zhang, J. (2020b). Shallow gas in the Holocene mud wedge along the inner East China Sea shelf. *Mar. Petrol. Geol.* 114, 104233. doi:10.1016/j.marpetgeo.2020.104233
- Dondurur, D., Cifci, G., Drahor, M. G., and Coskun, S. (2011). Acoustic evidence of shallow gas accumulations and active pockmarks in the Izmir Gulf, Aegean sea. *Mar. Pet. Geol.* 28, 1505–1516. doi:10.1016/j.marpetgeo.2011.05.001
- Feng, J., Zhao, T., Sun, Y., Gao, X., and Li, P. (2017). Analysis on acoustic detection of geo-hazard factors in Bohai Strait. *Comput. Tech. Geophys. Geochem. Explor.* 37 (1), 96–102.
- Liu, D., Hu, T., Huang, P., and Ji, Y. (2014). Classification and distribution of marine geo-hazards factors in Zhoushan islands. *Trans. Oceanol. Limnol.* 3, 153–160.
- Liu, Z., and Xia, D. (2007). *Tidal current sediment body in offshore China*. Beijing: Ocean Press.
- Qiao, P., Chen, S., Zhang, Y., Xu, C., Kong, X., and Yu, K. (2022). Types and formation mechanism of main geological hazards in the Western continental shelf area of the East China Sea. *J. Hebei Geo Univ.* 45 (3), 63–72.
- Qiu, J., Liu, J., Kong, X., Zhang, Y., Yue, B., Zhang, J., et al. (2012). Characteristics and distribution of geo-hazard factors in the Western south Yellow Sea. *Mar. Geol. Quart. Geol.* 32 (1), 27–34. doi:10.3724/sp.j.1140.2012.01027
- Qiu, J., Liu, J., Yue, N., Wang, S., and Mai, D. D. (2018). Distribution and characteristics of hazardous geological features in the marine coastal and offshore areas of Zhejiang Province, East China Sea. *J. Ocean. Univ. China* 17 (6), 1318–1324. doi:10.1007/s11802-018-3671-y
- Shang, S., Fan, D., Yin, P., Vurr, G., Zhang, M., and Wang, Q. (2018). Late quaternary environmental change in Oujiang delta along the northeastern zhe-min uplift zone (southeast China). *Palaeogeogr. Palaeoclimatol. Palaeoecol.* 492, 64–80. doi:10.1016/j.palaeo.2017.12.012
- Sun, J., Zhang, W., and Jia, J. (2010). Hazardous geology and its relationship with environmental evolution in the Pearl River Estuary. *J. Trop. Oceanogr.* 29 (1), 104–110.
- Toth, Z., Spiess, V., and Jensen, J. (2014). Seismo-acoustic signatures of shallow free gas in the Bornholm basin, Baltic sea. *Cont. Shelf Res.* 88, 228–239. doi:10.1016/j.csr.2014.08.007
- Verweij, J., Nelskamp, S., Ten Veen, J., De Bruin, G., Geel, K., and Donders, T. (2018). Generation, migration, entrapment and leakage of microbial gas in the Dutch part of the Southern North Sea Delta. *Mar. Pet. Geol.* 97, 493–516. doi:10.1016/j.marpetgeo.2018.07.034
- Wang, H., Zhang, W., Li, C., Lei, W., Yang, D., Liang, T., et al. (2014). Single amino acid substitution of VP1 N17D or VP2 H145Y confers acid-resistant phenotype of type Asia1 foot-and-mouth disease virus. *Mar. Sci.* 38 (7), 103–111. doi:10.1007/s12250-014-3426-x
- Wang, J., Zhang, G., Chen, D., Wang, X., Wang, Z., Dong, D., et al. (2019). Geological hazards in lingshui region of qiongdongnan basin: Type, distribution and origin. *Mar. Geol. Quart. Geol.* 39 (4), 87–95.
- Wang, Z., Xu, H., Zhan, Q., Saito, Y., He, Z., Xie, J., et al. (2010). Lithological and palynological evidence of late quaternary depositional environments in the subaqueous Yangtze delta, China. *Quat. Res.* 73, 550–562. doi:10.1016/j.yqres.2009.11.001
- Weschenfelder, J., Klein, A., Green, A., Aliotta, S., de Mahiques, M., Neto, A., et al. (2016). The control of palaeo-topography in the preservation of shallow gas accumulation: Examples from Brazil, Argentina and south Africa. *Estuar. Coast Shelf Sci.* 172, 93–107. doi:10.1016/j.ecss.2016.02.005
- Wu, X., Xing, L., Zhang, T., and Xiang, R. (2018). Mid-late Holocene changes in sedimentary organic matter on the inner shelf of the East China Sea. *J. Asian Earth Sci.* 154, 248–254. doi:10.1016/j.jseaes.2017.12.006
- Xu, H., Wang, J., and Zhou, H. (2017). Preliminary study on the mechanism of the erosion-deposition adjustment in the tidal inlet out of the Oujiang Estuary. *J. Mar. Sci.* 35 (2), 33–43.
- Xu, X., O'Reilly, S., Griffin, W., Wang, X., Pearson, N., and He, Z. (2007). The crust of cathaysia: Age, assembly and reworking of two terranes. *Precambrian Res.* 158, 51–78. doi:10.1016/j.precamres.2007.04.010
- Yang, J., ChenLiuXu, Z., Song, W., Wang, S., et al. (2022). Acoustic stratigraphy of the quaternary in the south of the Oujiang River estuary. *Mar. Geol. Front.* 38 (8), 11–19.
- Ye, W., Zhang, G., Zhu, Z., Huang, D., Han, Y., Wang, L., et al. (2016). Methane distribution and sea-to-air flux in the East China sea during the summer of 2013: Impact of hypoxia. *Deep Sea Res. Part II Top. Stud. Oceanogr.* 124, 74–83. doi:10.1016/j.dsr2.2015.01.008
- Ye, Y. (2011). Review of the development of marine hazard geology and its future prospects. *J. Mar. Sci.* 29 (4), 1–7.
- Zhang, G., Zhang, J., Liu, S., Ren, J., Xu, J., and Zhang, F. (2008). Methane in the changjiang (Yangtze River) estuary and its adjacent marine area: Riverine input, sediment release and atmospheric fluxes. *Biogeochemistry* 91, 71–84. doi:10.1007/s10533-008-9259-7
- Zhang, Z., Zhou, L., Chen, Y., Liang, L., and Bao, X. (2020). Study on the accumulative effects of reclamation on hydrodynamic force in Qujiang estuary. *Trans. Oceanol. Limnol.* 2, 64–71.
- Zheng, J. (2010). *Study on dynamical characteristics of the water environment during estuarine reclamation*. Beijing: Tsinghua University.
- Zhuang, Z., Cao, L., Liu, S., and Hu, G. (2008). Activity level and balance signs of subaqueous dunes (waves) in the continental shelf. *J. Ocean. Univ. China* 38 (6), 1001–1007.